ELSEVIER

Journal of Nuclear Materials 274 (1999) 66–77

journal of nuclear materials

www.elsevier.nl/locate/jnucmat

Radiation damage effects in zirconia

K.E. Sickafus [a,*], Hj. Matzke [b], Th. Hartmann [a], K. Yasuda [c], J.A. Valdez [a], P. Chodak III [d], M. Nastasi [a], R.A. Verrall [e]

[a] *Materials Science and Technology Division, Los Alamos National Laboratory, Los Alamos, NM, USA*
[b] *European Commission, Joint Research Centre, Institute for Transuranium Elements, Karlsruhe, Germany*
[c] *Department of Nuclear Engineering, Kyushu University, Fukuoka, Japan*
[d] *Technology and Safety Assessment Division, Los Alamos National Laboratory, Los Alamos, NM, USA*
[e] *Fuel and Fuel Cycle Division, CANDU Technology Development, AECL, Chalk River Laboratories, Chalk River, Ontario, Canada*

Abstract

The evolution of radiation-induced damage in fully-stabilized, cubic zirconia (FSZ) (Y, Ca and Er dopants acting as stabilizers) and in pure, unstabilized, monoclinic zirconia, was investigated using Rutherford backscattering spectrometry and ion channeling (RBS/C), along with X-ray diffraction and transmission electron microscopy (TEM). FSZ crystals were irradiated with 340–400 keV Xe^{++} ions and at temperatures ranging from 170 to 300 K, or with $^{127}I^{+}$ ions (72 MeV) at temperatures ranging from 300 to 1170 K. No amorphization of zirconia was found under any irradiation condition, though in the case of 72 MeV I^{+} ion irradiations, the irradiation-induced defect microstructure was observed to produce dechanneling effects in RBS/C measurements that reach the 'random' level. Damage accumulation in Xe-ion irradiation experiments on FSZ crystals was found to progress in three stages: (1) formation of isolated defect clusters; (2) a transition stage in which damage increases rapidly over a small range of ion dose, due to the linking of dislocations and defect clusters; and (3) a 'saturation' stage in which damage accumulation is retarded or increases only slowly with ion dose. The FSZ crystal composition does not seem to alter significantly the dose-dependence of these damage stages. Unstabilized, monoclinic ZrO_2 was observed to transform to a higher symmetry, tetragonal or cubic phase, upon 340 keV Xe^{++} ion irradiation to Xe fluences in excess of 5×10^{18} m^{-2} (dose equivalent, ~ 2 displacements per atom or dpa) at 120 K. This transformation was accompanied by a densification of the ZrO_2 phase by $\sim 5\%$. No amorphization of the pure ZrO_2 was observed to a Xe^{++} ion fluence equivalent to a peak displacement damage level of about 680 dpa.

1. Introduction

Advanced nuclear fuel design concepts have recently focused attention on so-called 'inert-matrix' fuels (e.g., see Refs. [1–7]). These fuels burn plutonium or other actinides such as americium instead of uranium. They have the dual advantage that they do not breed plutonium or higher actinides (Am, Cm) during burnup and that the actinide inventory in the spent fuel is significantly reduced compared to conventional urania or mixed oxide (MOX) [1] fuels. Of the candidate non-fertile diluents for inert matrix fuels, zirconia has received much attention (see, for instance [4,8,9]). This high temperature refractory oxide is attractive because actinides are readily incorporated in its structure and because it possesses high chemical durability and excellent radiation stability characteristics. The purpose of this paper is to examine further the radiation behavior of cubic zirconia and its monoclinic polymorph. First some additional introductory remarks are necessary.

* Corresponding author: Tel.: +1-505 665 3457; fax: +1-505 667 6802; e-mail: kurt@lanl.gov

[1] MOX or mixed oxide fuels are mixtures of urania (UO_2) and plutonia (PuO_2).

0022-3115/99/$ – see front matter
PII: S0022-3115(99)00041-0

Zirconia is the common name for zirconium dioxide (ZrO_2), a polymorphic oxide that exists in three different crystal structures below its melting point of 2950 K: (1) a high-temperature cubic (c) phase, isostructural with fluorite (CaF_2) (space group Fm $\bar{3}$m) from 2640 to 2950 K; (2) an intermediate temperature tetragonal (t) phase (space group $P4_2/nmc$) from 1440 to 2640 K; and (3) below 1420 K, the low temperature, naturally occurring monoclinic (m) form of zirconia (same as the mineral baddeleyite, space group $P2_1/c$) [10–12]. The m-ZrO_2 phase is a distorted fluorite structure ($a = 514.6$ pm, $b = 521.3$ pm, $c = 531.1$ pm, $\beta = 99.2°$ [13]), as is the t-ZrO_2 phase (for the primitive t unit cell, $a = 364$ pm, $c = 527$ pm [13]), the latter having the appearance of being in tension along the c-axis ($a^* = 515$ pm, $c^* = 527$ pm, for the non-conventional t unit cell) compared to c-ZrO_2 ($a = 509$ pm [13]). The polymorphism of zirconia is particularly interesting in that each successive high-temperature structure is more symmetric (as may be expected), yet more dense ($V^m_{\text{unit cell}} = 0.1407$ nm^3, $V^t_{\text{unit cell}} = 0.1397$ nm^3, $V^c_{\text{unit cell}} = 0.1319$ nm^3).

An important property of zirconia is that when certain aliovalent cations are substituted for Zr^{4+} in ZrO_2 (for instance, Mg^{2+}, Ca^{2+}, or Y^{3+}), they effect stabilization of the cubic fluorite structure from room temperature to the melting point of the compound [12]. Cubic solid solutions produced in this way (ZrO_2–MgO, ZrO_2–CaO, or ZrO_2–Y_2O_3) are commonly referred to as fully-stabilized zirconia (FSZ) compounds. Somewhat smaller additions of these same oxides lead to compounds referred to as partially-stabilized zirconia (PSZ), which are characterized by the presence of both c and t (and sometimes m) forms of zirconia [12]. In the context of nuclear fuels, the cubic phase of zirconia is of interest because compounds such as urania (UO_2), plutonia (PuO_2), ceria (CeO_2), and thoria (ThO_2) crystallize in the fluorite structure and so are isostructural with cubic ZrO_2 (e.g., [14,15]).

The concept of a zirconia matrix fuel is not new. A 1962 Westinghouse Electric Co. report documents irradiations performed on 94 fuel elements in the ZrO_2–UO_2 composition field [16]. The elements were irradiated at the National Research Universal (NRU) reactor at Chalk River, Ontario, and the National Reactor Testing Station in Idaho. A 1966 report describes a ZrO_2–UO_2–CaO fuel burned in the Power Burst Facility (PBF) at the Idaho National Engineering Facility with no fuel rod failures for temperatures to 2420 K [17]. Between 1969 and 1974, a ternary fuel consisting of 57 ZrO_2–38 UO_2–5 CaO (wt%) was successfully irradiated in the Shippingport pressurized water reactor (PWR) in Pennsylvania [18]. And a light water breeder reactor (LWBR) program tested a ternary ZrO_2–UO_2–CaO fuel and achieved high burnup without fuel failure [18]. In 1965, a study was conducted to identify an inert diluent for UO_2–PuO_2 fuel mixtures [19]. ZrO_2 was selected because of its low neutron absorption cross-section, such that it behaves as an innocuous material in a reactor environment. The neutronic behavior of elemental zirconium in reactor environments is well known, as it is the majority constituent in *Zircaloy*, a corrosion-resistant fuel cladding material with small neutron capture cross-section. Zircaloy has been used in thermal reactors for more than 30 yr now [20].

As a fuel matrix, zirconia must survive energy deposition due to neutron exposure, gamma and beta radiation, fission fragment damage, and self-irradiation from alpha decay of Pu and other actinides. To date, neutron and fission fragment damage studies have been performed on various forms and compositions of zirconia, and alpha decay damage has been simulated in ion irradiation experiments. At least one electron irradiation damage study on zirconia has also been reported [21].

The fist neutron irradiation experiment on zirconia was reported by Klein in 1955 [22]. Klein irradiated a pressed disk of PSZ consisting of both m- and c-ZrO_2 phases, and an FSZ (c-ZrO_2) disk to a fast-neutron ($E_n > 0.1$ MeV) fluence of 2×10^{24} m^{-2} or about 0.2 displacements per atom (dpa). [2] In the PSZ sample, the monoclinic phase was seen to 'disappear' by this neutron dose, while the cubic phase remained intact. In the FSZ sample, the lattice parameter of the cubic phase was observed to increase by 0.28%.

Wittels and Sherrill [24] reported in 1956 on a fast neutron irradiation of natural baddeleyite (m-ZrO_2) powder samples to a neutron fluence of 9.4×10^{23} m^{-2} (0.094 dpa) at 373 K. They observed that by this dose, more than 90% of the m-ZrO_2 transformed into the high-temperature c-ZrO_2 phase. Further exposure to neutrons caused complete disappearance of the monoclinic X-ray reflections [25]. The lattice parameter of the irradiation-induced c-ZrO_2 was reported to be appreciably greater than that of FSZ, suggesting that the irradiated zirconia contained a relatively high concentration of lattice defects [25].

But in subsequent neutron irradiation experiments using synthetic crystals and powders of pure ZrO_2, Wittels and Sherrill could not reproduce the m $\rightarrow$ c transformation, even at neutron fluences four times the original dose [26]. Wittels and Sherrill discovered that the transformation they observed previously in natural baddeleyite was due not to neutron damage, but to

[2] In this paper, fast-neutron induced displacement damage is estimated assuming an equivalence of 1 dpa per 10^{25} m^{-2} neutron fluence, $E_n > 0.1$ MeV. Comments regarding the validity of this approximation for oxide ceramics are given elsewhere [23].

fission fragment damage induced by fissioning of uranium and thorium impurities in the baddeleyite (concentrations of 3550 and 39.2 ppm, respectively) [26]. They proposed that a 'fission spike' mechanism is responsible for the m → c transformation in ZrO_2.

Adam and Cox [27,28] confirmed that pure, m-ZrO_2 does not undergo an m → c transformation under neutron bombardment, but their results indicated further that the transformation is only possible when impurities are present to aid the heterogeneous nucleation of the cubic phase. In the absence of impurities, not even fission fragment damage could effect an m → c transformation in ZrO_2. Adam and Cox also noted that the alleged m → c transformation in natural baddeleyite was actually a monoclinic to tetragonal (m → t) transformation.

Nevertheless, stress measurements in fission-fragment-irradiated pure m-ZrO_2 single crystals implied that an m → c (or m → t) transformation takes place upon irradiation to an integrated fission fragment fluence of $\sim 5 \times 10^{18}$ m^{-2} [29]. Specifically, the authors of this study observed a significant contraction of the zirconia crystals at this dose, which is best explained by an irradiation-induced phase transformation to the denser tetragonal or cubic phase.

The m → c (or m → t) transformation has special significance in relation to zirconium alloy fuel claddings. Were the surface of zircaloy cladding to experience such transformations during irradiation, the concomitant volume change would lead to cracking of the native oxide coating. This must necessarily increase the corrosion rate of the underlying metal [30]. This effect was confirmed in oxide films on Zr–5%V alloys exposed to an integrated fission fragment fluence of $\sim 7.5 \times 10^{18}$ m^{-2}, where a 90% m → c transformation was observed at this fluence using glancing-angle X-ray diffraction [31]. This effect led Johnson [30] to develop a Zr alloy with a cubic zirconium oxide coating for zircaloy, in order to prevent phase transformation of the oxide coating under irradiation.

In 1960, results from in-pile reactor irradiation tests of ZrO_2–UO_2 alloys were first reported [32]. Two compositions were tested: (1) cubic UO_2–20ZrO_2 (wt%); and (2) ZrO_2–13CaO–17UO_2 (wt%) (a mixture of a zirconia-rich tetragonal phase and a urania-rich cubic phase). Neither sample exhibited measurable volume swelling, while X-ray diffraction patterns obtained from both samples were unchanged following neutron exposures of 1.5×10^{23} and 6.8×10^{23} m^{-2}, respectively (these neutron fluences likewise induced fission events with fission fragment concentrations given by 2.8×10^{25} and 1.4×10^{26} m^{-3}, respectively). X-ray diffraction from the cubic UO_2–20ZrO_2 sample did reveal an initial lattice expansion from $a = 537.1$ pm to $a = 538.2$ pm at fission fragment concentration 2×10^{22} m^{-3}, followed by a contraction of the cell edge to $a = 534.3$ pm at fission fragment concentration 1.4×10^{25} m^{-3}.

Volume swelling was observed in neutron-irradiated yttria cubic stabilized zirconia (Y-FSZ) samples by Clinard et al. in 1977 [33]. Specifically, they observed a volume expansion of 1.76% at 875 K following a fast-neutron (>0.1 MeV) exposure of 3.8×10^{25} m^{-2} (3.8 dpa). However, they observed no swelling at an irradiation temperature of 1025 K to a neutron fluence of 2.8×10^{25} m^{-2} (2.8 dpa), nor more than 0.21% swelling at 640 K to a neutron fluence of 4.4×10^{25} m^{-2} (4.4 dpa). Nevertheless, the observed swelling behavior of Y-FSZ at intermediate temperatures indicates potential concern for pellet stability under nuclear fuel irradiation conditions.

More recent efforts to assess the radiation damage behavior of zirconia have emphasized ion irradiation studies. Most of these experiments have involved attempts (without success) to amorphize FSZ. Xenon ion irradiations of Y-FSZ (5–10 mol% Y_2O_3) to very high doses indicate no propensity for amorphization (for irradiation temperatures as low as 20 K), nor are other crystal phase transformations observed (240 keV Xe^+, [34]; 400 keV Xe^{++}, [35]; 1.5 MeV Xe^+ and 60 keV Xe^{++}, [36]; 400 keV Xe^{++}, [37]; 60 keV Xe^{++}, [38]; 370 keV Xe^{++}, [39]). Under cryogenic and ambient irradiation conditions, no amorphization was observed in zirconia to peak atomic displacement damage levels of at least 100 dpa [34,35,37]. This peak dose is far greater than that necessary to amorphize magnesium aluminate spinel ($MgAl_2O_4$), itself a highly radiation tolerant material [40]. Fleischer et al. [34,41] also observed a substantial hardening (15%) of Y-FSZ at low Xe ion fluences followed by softening to a level 15% below the unirradiated value at higher Xe doses. Other ion irradiation studies showing significant changes in hardness or fracture toughness of zirconia include Al^+ and Zr^+ irradiations of Y-FSZ [42] and Ar^+ [43] or As^+ [44] irradiations of Y-PSZ. Their observations were made using the Knoop and Vickers microindentation techniques. On the contrary, using the nanoindentation technique, Sickafus et al. [39] measured very little change in hardness (or elastic modulus) for Y-FSZ with increasing Xe ion fluence.

Finally, a recent report discussed results of ion irradiations of Y-FSZ single crystals using 72 MeV I^+ ions [45]. The intent of these irradiations was to simulate fission fragment damage in zirconia. For I^+ fluences ranging from 0.1×10^{19} m^{-2} and irradiation temperatures from 300 to 1770 K, these irradiations resulted in significant microstructural alterations to the crystals, but no amorphization of Y-FSZ was observed.

In this paper, we report new ion irradiation results for both FSZ (c-ZrO_2) samples with varying composition and for unstabilized, m-ZrO_2.

Table 1
Compositions of FSZ single crystals used for ion irradiation damage studies

X-FSZ	ZrO_2 (mol%)	Y_2O_3 (mol%)	Er_2O_3 (mol%)	CaO (mol%)	HfO_2 (mol%)
Y-FSZ	89.5	9.5	–	–	1.0
Ca-FSZ	85.0	–	–	14.1	0.9
(Y, Er)-FSZ	86.6	11.1	1.3	–	1.0

2. Experimental procedure

The cubic-stabilized zirconia crystals used in this study were obtained from Zirmat Corp. (P.O. Box 365, N. Billerca, MA 01862, USA). FSZ crystals contained either Y_2O_3 (Y-FSZ) or CaO (Ca-FSZ) to stabilize the cubic, fluorite structure. One yttria-stabilized crystal also contained Er_2O_3 as a rare-earth dopant (heretofore, this composition is referred to as (Y, Er)-FSZ). Compositions of the FSZ crystals used in these experiments, determined using an electron microprobe are indicated in Table 1.

Crystals were aligned to an $\langle 0\,0\,1\rangle$-orientation using a Laue back-reflection X-ray diffraction camera, then cut to dimensions of approximately 10 mm × 10 mm × 1 mm. [3] Each sample was then polished on one side to a mirror finish.

Polycrystalline samples of synthetic m-ZrO_2 (same structure as the mineral baddeleyite) were also prepared for irradiation, using 99.978% 'Puratronic' grade ZrO_2 powder from Alfa AESAR (30 Bond Street, Ward Hill, MA 01835, USA). Monoclinic ZrO_2 powder was cold-pressed into 10 mm diameter by 1 mm thick disks using a static load of about eight metric tons.

Samples were irradiated with 340–400 keV Xe^{++} ions using a 200 kV ion implanter in the Ion Beam Materials Laboratory (IBML) at Los Alamos National Laboratory (LANL). The samples were tilted to about 15° with respect to the incident ion beam, in order to minimize ion channeling effects during the irradiations. Xe fluences ranged from 1×10^{17} to 2×10^{21} m^{-2}. The sample stage was cooled to a temperature of 120–170 K by liquid nitrogen conduction cooling. Additional irradiations were performed with the sample at ambient temperature (300 K). Temperature excursions during irradiations were about ±5 K, as measured using a thermocouple attached to the sample stage. The Xe^{++} ion flux was maintained at 1×10^{17} m^{-2} s^{-1}, corresponding to a peak damage rate of about 0.03 dpa s^{-1} for zirconia.

A similar set of zirconia crystals was irradiated with 72 MeV $^{127}I^+$ ions in the TASSC accelerator facility at Chalk River Laboratory. Irradiations were performed over the I^+ fluence range $0.1–5\times10^{19}$ m^{-2}, at temperatures of 300, 770 and 1170 K. The I^+ ion flux was maintained at 1×10^{16} m^{-2} s^{-1}. The irradiated sample area was about 2 mm in diameter.

Radiation damage accumulation in single crystal FSZ samples was assessed using Rutherford backscattering spectrometry and ion channeling (RBS/C) techniques. RBS/C analyses of Xe^{++} ion implanted crystals used a 2 MeV He^+ ion beam aligned along the $\langle 0\,1\,1\rangle$ axial direction in the in situ analysis chamber at LANL (see Yu et al. [46] for experimental details). These samples were coated with a 20 nm thick layer of carbon to avoid surface charging problems during ion beam analysis. I^+ ion implanted samples were examined by RBS/C at INFP, FZK Karlsruhe, using a 2 MeV He^+ beam aligned along an $\langle 0\,0\,1\rangle$-orientation. Samples were coated with thin layers of gold, except where small ($\sim$ 2 mm diameter) masks were placed over the areas of interest, again to minimize charging problems during RBS/C analyses. Volume swelling in the I^+ irradiated samples was also measured using a Rodenstock RM600-S laser profilometer.

The projected range of 370 keV Xe^{++} ions (an average energy used in these experiments) and 72 MeV I^+ ions as well as the number of atomic displacements produced per ion in zirconia were estimated from Monte Carlo simulations using the TRIM binary collision code [47] (specifically, using SRIM, i.e., TRIM-96). For calculations, a density of 5.96×10^3 kg m^{-3} was used (according to [13], this is the density of $Zr_{0.85}Y_{0.15}O_{1.93}$, Y-FSZ, which is close to the composition of most of our samples). Also, a threshold displacement energy of 40 eV was assumed for all elements. TRIM simulation results are shown in Table 2.

Due to ionization mechanisms, the swift 72 MeV I^+ ions are subjected to large electronic losses over much of their range. This electronic loss component of the stopping decreases approximately linearly over most of the ion range.

The irradiated monoclinic ZrO_2 samples were analyzed by X-ray diffraction using a Scintag XDS 2000 with theta–theta geometry using $CuK\alpha_1$ radiation, and a graphite secondary monochromator. The data were taken in Bragg reflection geometry, and the instrument was operated in step-scan mode with 0.01° 2θ steps and 5 s step-time. Rietveld structure analyses were

[3] We also used samples that were cut to a thickness of 0.5 mm, but these samples tended to fracture during the 72 MeV I^+ irradiations, presumably due to thermal shock.

Table 2
Calculated ion transport parameters for 370 keV Xe^{++} and 72 MeV I^{+} ion irradiations of zirconia (based on the TRIM code)

Ion species	Longitudinal range (nm)	Longitudinal straggling (nm)	Peak implantation concentration per 10^{19} m^{-2} Ion fluence (at.%)	Total atomic displacements per ion (ion^{-1})	Peak displacement damage per 10^{19} m^{-2} Ion fluence (dpa)	Electronic stopping power at crystal surface (keV nm^{-1})
370 keV Xe^{++}	77	27	0.185	2300	3.4 (depth $\sim$ 50 nm)	1.3
72 MeV I^{+}	6.8×10^3	510	0.014	3.2×10^4	1.5 (depth $\sim 6.7 \times 10^3$nm)	19

performed using the GSAS package [48]. No internal standard was added to the ZrO_2. To refine diffractometer constants, the structural parameters of baddeleyite were fixed for the first refinement cycles.

These same ZrO_2 samples were then impregnated with epoxy and prepared in cross-section for examination by transmission electron microscopy (TEM). The radiation-induced microstructures were examined in a Philips CM-30 electron microscope operating at 300 kV. Bright-field (BF) imaging and microdiffraction techniques were used for analyses.

3. Results

3.1. Fully-stabilized cubic zirconia

Lattice damage evolution in Xe-irradiated FSZ single crystals were quantified using RBS/C analysis techniques. A useful damage accumulation parameter by ion channeling is χ, a ratio between the direct backscattered He ion yield with the crystal aligned in a low index crystallographic orientation, and the backscattered He ion yield with the crystal aligned in a 'random' (high index) orientation. Typically, χ is an integrated ion yield ratio, for a backscattered He ion energy range corresponding to depths in the crystal where lattice defects due to irradiation damage reside. Fig. 1 shows a plot of χ as a function of Xe ion dose for cubic zirconia crystals Y-FSZ, Ca-FSZ, and (Y, Er)-FSZ (Table 1). This data was obtained from RBS/C spectra (not shown) similar to results obtained by Yu et al. [35] and Yasuda et al. [37]. χ was calculated using a He backscattered energy range between 1.5 and 1.6 MeV, where a peak in RBS/C backscattering spectra is observed due to subsurface radiation-induced defects from Xe-ion implantation.

In each FSZ crystal, the damage accumulation parameter χ is observed to rise slowly over a range of about two orders of magnitude ion fluence, then to rise rapidly over less than an order of magnitude fluence, and finally to saturate or rise slowly for higher ion fluences. These regions are denoted in Fig. 1 by the labels, Stages 1–3. The peak displacement damage estimated using TRIM is also shown in Fig. 1, and for all FSZ crystals, Stage 2 occurs between 3 and 10 dpa. Data in Fig. 1 were obtained from samples irradiated under ambient conditions (300 K), but χ_{min} results obtained from each sample under cryogenic irradiation conditions (170 K) are nearly identical to those shown in Fig. 1.

In a previous study, TEM experiments were performed on FSZ samples taken from Stages 1 and 3 [37]. In the middle of Stage 1, tiny (<5 nm diameter) isolated defect clusters were observed, while in Stage 3 samples, high densities of overlapping microstructural defects, primarily dislocations and dislocation clusters, were observed. Apparently, Stage 2 denotes a transition in the radiation damage evolution from the formation of isolated microstructural defect clusters to the linking or interconnecting of extended lattice defects. According to Fig. 1, this transition occurs at a similar displacement

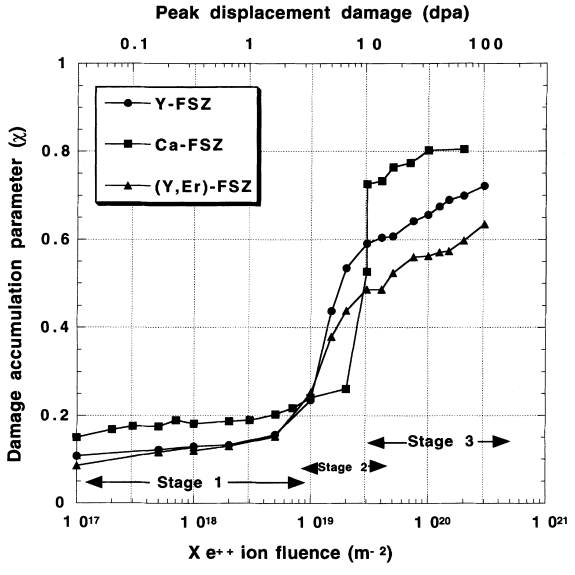

Fig. 1. Damage accumulation parameter, χ, versus Xe^{++} ion fluence, based on RBS/C measurements of FSZ samples irradiated at ~170 K using 400 keV Xe^{++} ions. The upper abscissa on the graph represents the maximum number of displacements per atom (dpa) effected by 400 keV Xe^{++} ions at the corresponding ion fluence on the lower abscissa. This maximum occurs at a depth of ~50 nm in FSZ.

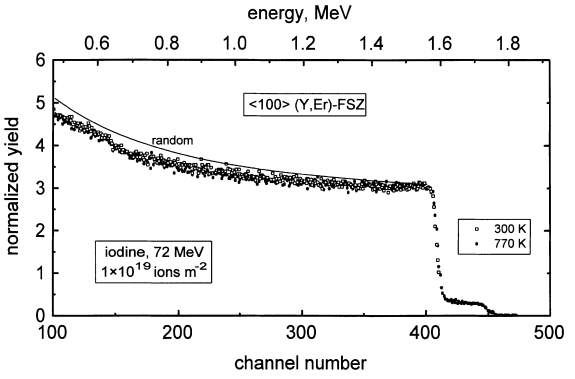

Fig. 2. RBS/C spectra obtained from sample (Y, Er)-FSZ irradiated with 72 MeV $^{127}I^+$ ions to a fluence of 1×10^{19} ions m^{-2} at either ambient temperature (300 K) or at 770 K. Spectra show the backscattered yield of 2 MeV He^+ ions as a function of backscattered ion energy. A 'random' RBS spectrum from (Y, Er)-FSZ is also shown for comparison with the channeling spectra. The leading edge in the spectra (~1.7 MeV) represents scattering from Hf (an impurity in the FSZ crystals) and Er (an intentional dopant in these samples). The prominent rise in yield at lower energy (~1.6 MeV) is due to surface scattering from Zr.

damage level (~ 3 dpa) in Y-FSZ and (Y, Er)-FSZ; by comparison, it is slightly delayed (5–9 dpa) in Ca-FSZ. However, this discrepancy may simply reflect the fact that the FSZ density used in TRIM calculations was that of yttria-stabilized zirconia rather than calcia-stabilized zirconia.

72 MeV I^+ irradiations produced damage levels in FSZ considerably higher than the Xe^{++} irradiations. Fig. 2 shows RBS/C spectra from (Y, Er)-FSZ samples irradiated to an I^+ fluence of 1×10^{19} m^{-2} at 300 and 770 K. Independent of irradiation temperature, the channeling spectra are very similar to the 'random' spectrum in Fig. 2, indicating that χ_{min}, as defined earlier, is approximately unity for these irradiation conditions. Dechanneling to the random level is usually indicative of an amorphization (or metamict) transformation. However, previous TEM observations of similar I^+ irradiated FSZ crystals found no evidence for such a transformation [45]. In that TEM study, a large concentration of dislocations and defect aggregates was observed in the irradiated volume of the FSZ crystals. These defects are apparently responsible for the observed dechanneling to the random level in the RBS/C measurements. An alternative explanation would be polygonization and formation of subgrains as is known to occur in the isostructural materials UO_2 and CeO_2 [49–51] and has been observed in Fe-implanted Y-FSZ [52].

If amorphization were to occur upon I^+ irradiation, it should be accompanied by a substantial volume change. Examples of this include observations of ~ 20% swelling in $CePO_4$ irradiated with 72 MeV I^+ to a dose of 1×10^{18} m^{-2} at 813 K [53], and ~ 30% free swelling in Al_2O_3 irradiated with 72 MeV I^+ to a dose of 1×10^{21} m^{-2} at 423 K [54]. In these studies, unilateral swelling due to ion irradiation was visible in profilometry scans as 'pop-out' features on the surface of the irradiated samples. Fig. 3 shows laser profilometry results obtained from FSZ crystals irradiated in this study. No pop-out features due to unilateral swelling are apparent, regardless of the composition of the sample or the temperature of irradiation. By contrast, Fig. 3(f) shows the surface of an I^+ irradiated spinel ($MgAl_2O_4$) crystal in which the two highest I^+ fluences have produced visible pop-out features. The diameter of the pop-out features in Fig. 3 (~ 2 mm) correspond to the diameter of the irradiating I^+ ion beam. Amorphization of a portion of the irradiated volume in spinel has been confirmed by TEM observation [55]. But, to date, no evidence for amorphization of FSZ has been obtained.

3.2. Unstabilized monoclinic zirconia

Fig. 4 shows portions of X-ray diffraction patterns obtained from a sample of pure, polycrystalline m-ZrO_2 and from a similar sample irradiated with 340 keV Xe^{++} ions to a fluence of 2×10^{21} m^{-2} at cryogenic temperature (120 K). All of the peaks in the unirradiated spectrum are indexed as reflections from monoclinic ZrO_2. However, following irradiation a new Bragg peak appears at $d = 296$ pm. This peak can be indexed as the $\langle 1\ 1\ 1 \rangle$ diffraction peak for a cubic Fm $\bar{3}$m unit cell with a lattice parameter of $a = 512.8$ pm. This is in reasonable agreement with lattice parameter measurements for cubic stabilized zirconia (for instance, $a = 513.9$ pm in $Zr_{0.85}Y_{0.15}O_{1.93}$, [13]). The large full-width at half-maximum (FWHM) of about 0.5° 2θ of this additional Bragg peak indicates rather poor crystallinity of the stabilized phase; as a result, it can also be indexed as $\langle 1\ 0\ 1 \rangle$ peak using a tetragonal $P4_2/nmc$ unit cell. No other peaks are visible in the irradiated spectrum to resolve this ambiguity.

This structural transformation was confirmed by TEM observations. Fig. 5 shows a BF TEM image of the Xe-irradiated m-ZrO_2 sample described above. The irradiated volume is viewed in cross-section with the ions incident from the top of the BF micrograph. A 170 nm thick layer of material exhibiting 'mottled' diffraction contrast is visible on top of a substrate made up of clearly visible grains (100–150 nm diameter) and voids. Microdiffraction patterns in Fig. 5 obtained from position (1) in the irradiated layer and (2) in the unirradiated substrate reveal a difference in structure. The substrate pattern is consistent with a monoclinic baddeleyite structure, while the implanted layer must be either tetragonal or cubic. Assuming a cubic structure, the principal reflections in microdiffraction pattern (1)

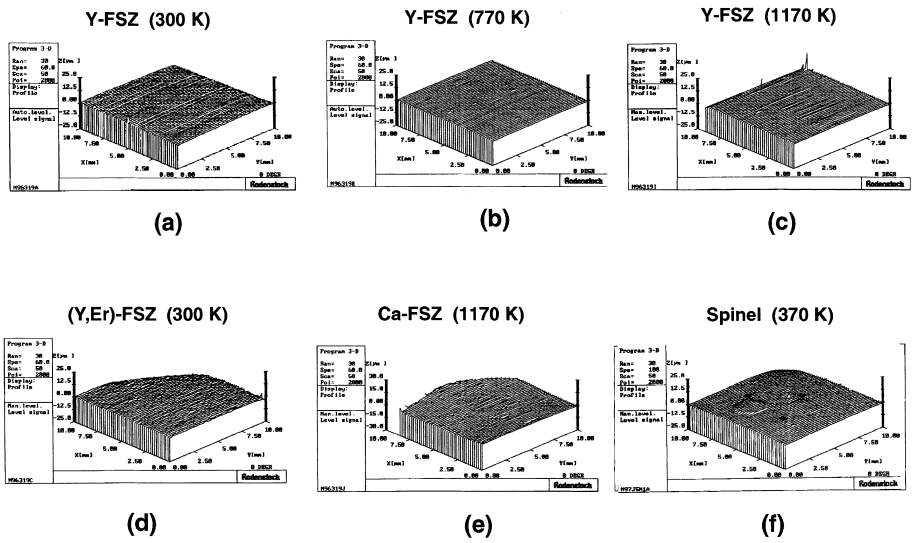

Fig. 3. (a–e). Laser profilometry traces from FSZ crystals irradiated with 72 MeV $^{127}I^{+}$ ions to 3 ion fluences: 0.1, 1, and 5×10^{19} m^{-2}. Irradiation temperatures are denoted adjacent to the profilometry traces. (f). Laser profilometry traces from a magnesium aluminate spinel ($MgAl_2O_4$) crystal irradiated with 72 MeV $^{127}I^{+}$ ions to 3 ion fluences: 0.5, 1, and 5×10^{19} m^{-2} at 370 K. Two 'popout' features (marked with arrows), each ~2 mm diameter, are visible in the traces. These are due to swelling of the spinel at the two highest irradiation doses. Lateral dimensions of scans are 10 mm × 10 mm with a vertical dimension of 25 μm. It is estimated that the resolution of this technique is ~0.1 μm. Thus, were the volume irradiated to exhibit unilateral swelling of ~2%, this would be visible as popout in the surface scan.

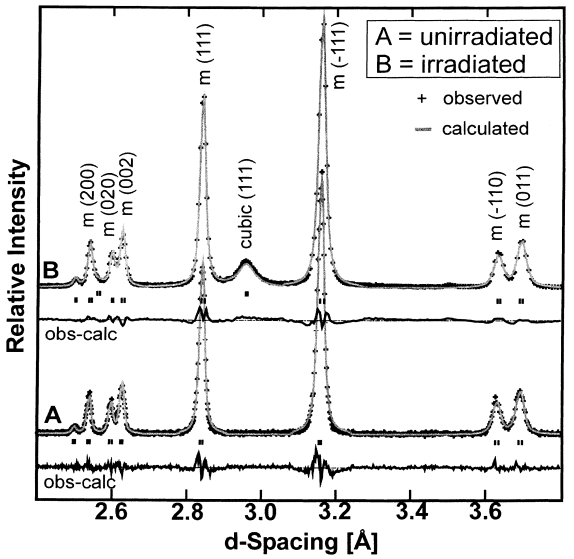

Fig. 4. X-ray diffraction pattern obtained from A: a sample of polycrystalline, unstabilized monoclinic ZrO_2; and B: a similar sample irradiated with 340 keV Xe^{++} ions to a Xe fluence of 2×10^{21} m^{-2} at cryogenic temperature (120 K). The solid curves (light gray) are Rietveld structure refinement fits to the diffraction data. The curves labeled 'obs-calc' show the refinement residues $\left(R_{\text{Bragg}} = [\sum |F_{\text{obs}}| - |F_{\text{cal}}|] / \sum |F_{\text{obs}}|\right)$. For both spectra, the residue is ~9%. Following irradiation, a new peak appears at $d = 2.96$ Å. This peak is labeled here as $\langle 1\,1\,1 \rangle$; this assumes cubic indexing for the new irradiation-induced zirconia phase.

are indexed as $\langle 1\,1\,1 \rangle$, $\langle \bar{3}\,3\,1 \rangle$, and $\langle 4\,\bar{2}\,0 \rangle$, which yields a beam direction of $\mathbf{B} = [\bar{1}\,\bar{2}\,3]$. The corresponding cubic lattice parameter derived by TEM is $a = 506$ pm, smaller than measured by X-ray diffraction, TEM results are unable to resolve the ambiguity regarding transformation to either a cubic or tetragonal unit cell. Table 3 shows measured lattice spacing ratios (based on microdiffraction results from Fig. 5) versus calculated lattice spacing ratios, assuming either a cubic or a tetragonal unit cell. Within experimental error, either assumption yields results in agreement with the observations.

4. Discussion

Our studies have shown that for Xe ions in the energy range 340–400 keV, lattice damage in FSZ (c-ZrO_2) crystals increases in three distinct stages. The first stage involves the formation of isolated defect clusters. The third stage is when radiation damage evolution is consummated with the interconnecting and overlapping of dislocations and extended lattice defects, but without a transformation to an amorphous (or metamict) phase. The second stage is a transition stage in which lattice damage appears to accumulate rapidly with ion fluence, as irradiation-induced defects begin to interact. Preliminary experiments presented here suggest that these observations may apply to all FSZ, independent of

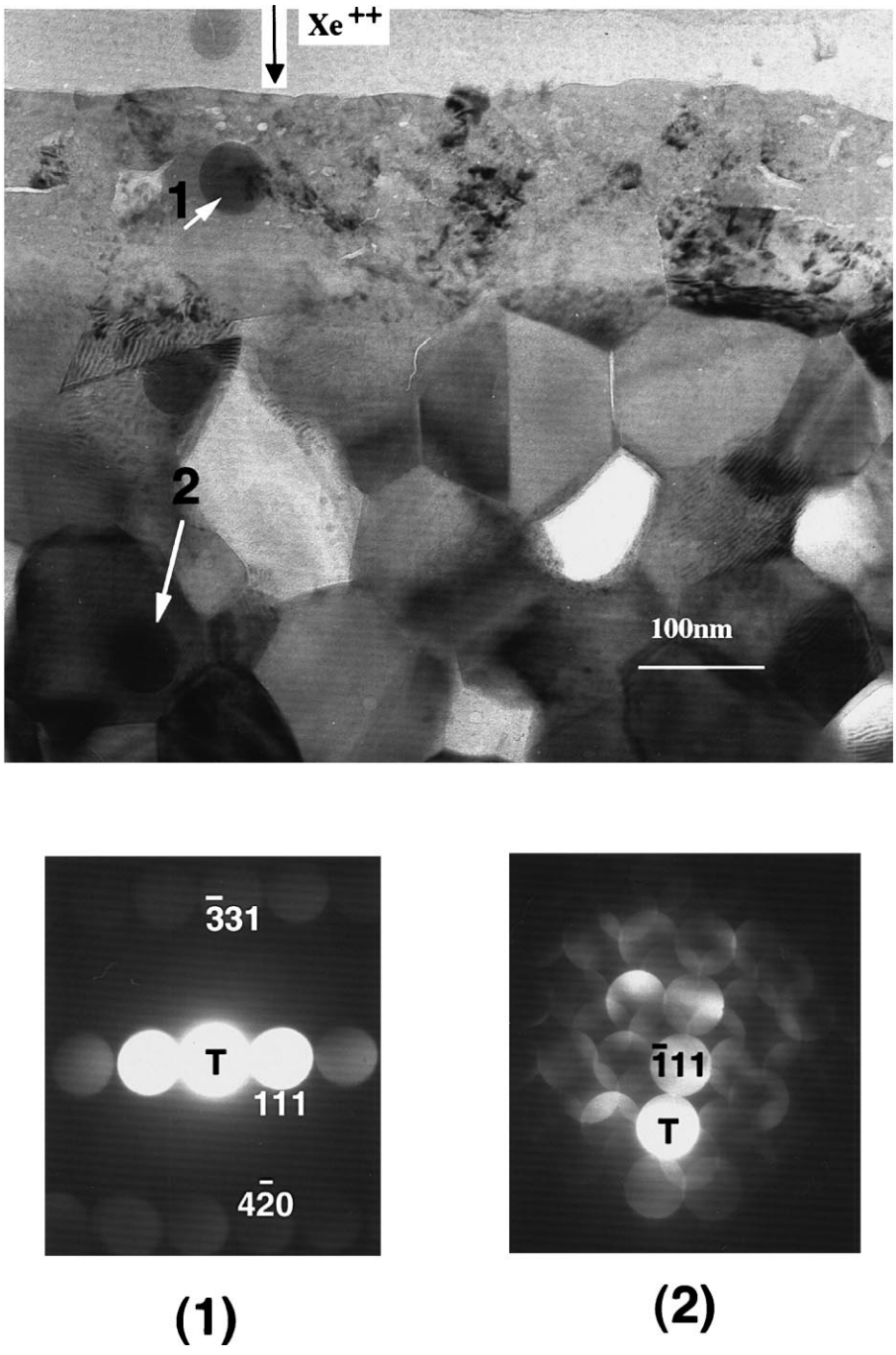

Fig. 5. The BF cross-sectional TEM micrograph of an unstabilized ZrO_2 sample irradiated with 340 keV Xe^{++} ions to a Xe fluence of 2×10^{21} m^{-2} at cryogenic temperature (120 K) (same as Fig. 4). A layer (~170 nm thick) at the top of the BF image shows a structure different than the polycrystalline substrate. Microdiffraction patterns (labeled (1) and (2)) were obtained from the irradiated layer at position 1 and in the substrate at position 2. Contamination spots are visible in the micrograph at these positions; this gives an indication of the size of the focused electron beam used for microdiffraction analysis. The reflections in pattern (1) are indexed assuming a cubic structure in the irradiated layer. Pattern (2) is consistent with a monoclinic ZrO_2 structure. The brightest reflection in this pattern is indexed as $\langle \bar{1}\,1\,1 \rangle$. The topmost layer visible in the BF image is an epoxy layer used for cross-sectional TEM preparation following irradiation. In the microdiffraction patterns, label 'T' indicated the transmitted beam.

Table 3
Measured interplanar (d) spacing ratios versus calculated ratios assuming either a cubic or tetragonal ZrO_2 unit cell. d_1, d_2, and d_3 correspond to the reflections in Fig. 5 labeled $\langle 1\ 1\ 1\rangle$, $\langle \bar{3}\ 3\ 1\rangle$, and $\langle 4\ \bar{2}\ 0\rangle$, respectively. d-ratios for the tetragonal unit cell assume a c/a ratio of 1.448 [13]

	Measured d-ratio	Cubic unit cell d-ratio	Tetragonal unit cell d-ratio		
$\frac{d_1}{d_2}$	2.52 ± 0.03	$2.517\left(\frac{d_{111}}{d_{331}}\right)$	$2.508\left(\frac{d_{101}}{d_{213}}\right)$	$2.533\left(\frac{d_{101}}{d_{301}}\right)$	
$\frac{d_1}{d_2}$	2.57 ± 0.03	$2.582\left(\frac{d_{111}}{d_{420}}\right)$	$2.554\left(\frac{d_{101}}{d_{114}}\right)$	$2.590\left(\frac{d_{101}}{d_{222}}\right)$	$2.602\left(\frac{d_{101}}{d_{310}}\right)$

composition. Other Xe ion irradiation studies using different FSZ compositions are in general agreement with our results. For instance, irradiations of ZrO_2–$10YO_{1.5}$–$5ErO_{1.5}$–$10ThO_2$ (at.%) cubic solid solutions showed no evidence for amorphization for 1.5 MeV Xe ions to a fluence of 2×10^{20} m^{-2} (~25 dpa) at 20 K [36], as well as microstructural evolution qualitatively similar to the description above.

For high radiation resistance, it is desirable to produce a material in which the onset of Stage 2 damage is delayed to the highest possible dose. Results presented here do not suggest that much variation in the onset of Stage 2 with composition is to be expected in FSZ materials. However, the initiation of Stage 2 damage in FSZ occurs at damage levels greater than in many ceramic materials (see, for instance, Sickafus et al. [56]) (exceptions include UO_2, ThO_2, UC, and UN [50,54]). So, FSZ appears to exhibit attractive radiation tolerance characteristics under moderate energy, heavy ion irradiation conditions. Such conditions are typical of certain fast neutron radiation damage conditions, as well as damage induced by heavy ion self-recoils associated with α-decay events. Much work is needed, however, to assess the temperature dependence of this three-stage radiation damage accumulation behaviour. Especially worrisome is the before-mentioned swelling peak at ~ 875 K observed in neutron irradiation experiments on Y-FSZ [33]. This temperature is reached and surpassed in light-water reactors. Consequently, care must be taken to assess FSZ swelling behavior under irradiation at high temperatures.

Swift heavy ions, such as the 72 MeV I^+ ions used in our experiments, appear to produce rather different damage in FSZ compared to lower energy, Xe ion irradiations. Though no amorphization is observed by these fission fragment simulation experiments, nor is volume swelling observed, the microstructural damage to FSZ induced by these highly-ionizing ions apparently is more severe than in moderate energy, heavy ion irradiations. Comparison of the RBS/C results presented here to previous work on Y-FSZ [45] suggests that fission fragment damage may also vary as a function of FSZ composition. Much more work is necessary to establish the relative resistance of FSZ to fission fragment damage.

Important results were also presented here regarding radiation damage evolution in unstabilized, m-ZrO_2. This material is observed to transform to a higher-symmetry phase, either t- or c-ZrO_2, upon exposure to heavy ion (Xe) irradiation. Our experiments indicate that this transformation begins at a Xe fluence of about 5×10^{18} m^{-2} for 340 keV Xe implantation at ~ 120 K, and is complete within an order of magnitude above this dose (between 2 and 20 peak dpa). But this transformed ZrO_2 structure persists to a larger Xe ion fluence, corresponding to a peak displacement damage level of about 680 dpa. As with FSZ samples, no amorphization is observed in unstabilized ZrO_2. Our results contradict an earlier study suggesting that a 'fission spike' mechanism is necessary to induce a structural transformation in monoclinic zirconia [24], although some sort of thermal spike mechanism may be operative in our experiments.

Heavy ion irradiation of monoclinic zirconia leads not only to stabilization of a structure with higher symmetry, but to higher density as well. Assuming the irradiation-induced transformation is from m-ZrO_2 to c-ZrO_2 (m → c), X-ray structure refinement values from data presented in Fig. 4 indicate that the ZrO_2 unit cell volume decreases from 0.1408 to 0.1348 nm^3, while the theoretical density increases by ~ 5%, from 5.8 to 6.1×10^3 kg m^{-3}. It was proposed previously by Wittels and Sherrill [24] and it seems plausible still, that this transformation is related to irradiation-induced interstitial point defects. To quote their words:

> The internal stresses about these defects and the proposed volume collapse which results are consistent with the unique temperature-structure behavior of zirconia.

Additional work is needed using different ion masses and energies to determine how important thermal spike effects are in inducing the m → c (or m → t) transformation (and to resolve debate regarding the structure of the transformation product, i.e. cubic or tetragonal). Nevertheless, it is important to realize that these experiments suggest that point defects produced by irradiation of pure, monoclinic ZrO_2, seem to 'self-stabilize' a higher symmetry phase of zirconia. It is now apparent

that the actual purpose of chemical additives to ZrO_2 is to prevent (if necessary) the volume change concomitant with an m → c (or m → t) transformation, rather than to enhance amorphization resistance or other adverse microstructural phenomena.

In summary, FSZ appears to exhibit impressive radiation tolerance and looks attractive as a material for application in high radiation environments. Moreover, pure m-ZrO_2 transforms to a phase resembling FSZ under low ion dose conditions and this structure persists to very high irradiation doses. Much more research is needed to fully understand the radiation damage behavior of zirconia. For instance, temperature effects are important and yet difficult to assess accurately due to the poor thermal conductivity of zirconia. Also, little or no work has been performed to determine the characteristics of microstructure in irradiated ZrO_2 (dislocation habit planes, faulted loop characteristics, unfaulting mechanisms, etc.). Additionally, effects due to high oxygen mobility at elevated temperature have not been examined. Even fundamental information regarding threshold energies for atomic displacements have not been studied either experimentally or theoretically. Since zirconia appears to be a promising material for either nuclear fuel or wasteform applications, many of these issues must now be addressed.

5. Conclusions

Radiation damage behavior in FSZ and in pure, unstabilized, monoclinic zirconia, was investigated using: (1) Rutherford backscattering spectroscopy and ion channeling techniques (RBS/C), (2) X-ray diffraction and (3) TEM. FSZ crystals were irradiated with Xe^{++} ions (energies ranging from 340 to 400 keV) at temperatures ranging from 170 to 300 K and with $^{127}I^{+}$ ions (72 MeV) at temperatures ranging from 300 to 1170 K. No amorphization of zirconia was found under any irradiation condition, though irradiation-induced defect concentrations became high enough to produce maximum ion dechanneling effects in RBS/C measurements (for 72 MeV I^{+} ions). Damage accumulation in Xe-irradiation experiments on FSZ crystals was found to progress in three stages: (1) an isolated defect cluster stage; (2) a transition stage in which damage increases rapidly over a small range of ion doses; and (3) a 'saturation' stage in which damage accumulation is retarded or increases only slowly with ion dose. FSZ crystal composition does not seem to alter significantly the dose-dependence of these damage stages.

Unstabilized, monoclinic ZrO_2 was observed to transform to a higher symmetry, cubic or tetragonal phase, upon 340 keV Xe^{++} ion irradiation to Xe fluences in excess of 5×10^{18} m^{-2} (dose equivalent, ~2 displacements per atom or dpa) at 120 K. This transformation was accompanied by a densification of the ZrO_2 phase by ~5%. No amorphization of the pure ZrO_2 was observed for a Xe ion dose equivalent to a peak displacement damage level of about 680 dpa.

Acknowledgements

The authors wish to thank M.G. Snow and R.G. Warren of Los Alamos National Laboratory (LANL) for providing electron microprobe analyses of the zirconia crystals used for this study, and C.J. Maggiore, J.R. Tesmer, M.G. Hollander, C.R. Evans, N. Borders and N. Yu (Texas Instruments), R. Fromknecht (INFP, FZK), and P.G. Lucuta (ACERAM Technol., Chalk River, Canada) for ion beam irradiation and analysis assistance, along with helpful discussions. Also, the authors from Los Alamos National Laboratory acknowledge the support provided by the Department of Energy, Office of Basic Energy Sciences, Division of Materials Sciences.

References

[1] Hj. Matzke, J. van Geel, Radwaste Mag. 3 (1996) 71.
[2] N. Cocuaud, E. Picard, R.J.M. Konings, A. Conti, Hj. Matzke, in: International Conference on Future Nuclear Systems: Global '97 (1997: Yokohama, Japan) (American Nuclear Society (Grange Park, IL), Pacifico Yokohama, Yokohama, Japan, October 5–10, 1997), vol. II, p. 1044.
[3] J.W. Sterbentz, C.S. Olsen, U.P. Sinha, Weapons-Grade Plutonium Dispositioning: vol. 4, Idaho National Engineering Laboratory, Idaho Falls, Idaho, DOE/ID-10422 (1993).
[4] C. Degueldre, U. Kasemeyer, F. Botta, G. Ledergerber, Mater. Res. Soc. Symp. Proc. 412 (1996) 15.
[5] P. Chodak III, M.J. Driscoll, N.E. Todreas, M.M. Miller, Destruction of Plutonium Using Non-Uranium Fuels in Pressurized Water Reactor Peripheral Assemblies, Massachusetts Institute of Technology, Cambridge, MA, MIT-NFC-TR-001 (1997).
[6] H. Akie, T. Muromura, H. Takano, S. Matsuura, Nucl. Technol. 107 (1994) 182.
[7] V.M. Oversby, C.C. McPheeters, C. Degueldre, J.M. Paratte, J. Nucl. Mater. 245 (1997) 17.
[8] C. Degueldre, U. Kasemeyer, F. Botta, Study of Plutonium Incineration in LWRs Employing an Uranium Free Fuel 'Inert Matrix – Burnable Poison – Actinide' Approach, Paul Scherrer Institut, Villigen, Switzerland, TM-43-95-12 (1995).
[9] G. Ledergerber, C. Degueldre, U. Kasemeyer, A. Stanculescu, J.M. Paratte, R. Chawla, Using Civilian Plutonium in LWRs with an Inert Matrix Fuel (IMF), Paul Scherrer Institut, Villigen, Switzerland, TM-43-97-40 and TM-41-98-06 (1998).

[10] A.H. Heuer, M. Rühle, in: N. Claussen, M. Rühle, A.H. Heuer (Eds.), Science and Technology of Zirconia II, The American Ceramic Society, Columbus, OH, 1984, vol. 12, p. 1.
[11] M. Rühle, A.H. Heuer, in: N. Claussen, M. Rühle, A.H. Heuer (Eds.), Science and Technology of Zirconia II, The American Ceramic Society, Columbus, OH, 1984, vol. 12, p. 14.
[12] R. Stevens, Zirconia and Zirconia Ceramics, Magnesium Elecktron Twickenham, United Kingdom, 1986.
[13] International Committee for Diffraction Data, Powder Diffraction File, Joint Committee on Powder Diffraction Standards, Philadelphia, PA, 1974 – present.
[14] J.G. Pepin, G.J. McCrathy, J. Am. Ceram. Soc. 64 (1981) 511.
[15] D.F. Carroll, J. Am. Ceram. Soc. 46 (1963) 194.
[16] B.F. Rubin, R.M. Berman, M.L. Bleiberg, The Irradiation Behavior of ZrO_2–UO_2 Fuels, Westinghouse Electric Corporation, Bettis Atomic Power Laboratory, Pittsburgh, PA, WAPD-264, UC-25: Metals, Ceramics, and Materials, TID-4500, 17th ed., 1962.
[17] H.R. Warner, Evaluation of Low Density Single-Phase Cubic ZrO_2 + UO_2 Fuels Stabilized with CaO, Westinghouse Electric Corporation, Pittsburgh, PA, WAPD-292, UC-25: Metals, Ceramics, and Materials, TID-4500, 46th ed., 1966.
[18] A. Boltax, A. Biancheria, A.L. Chang, P.J. Levine, D.K. Lincoln, Ternary Fuel Performance Data for the Special Water Reactor, Westinghouse Electric Corporation, Advanced Energy Systems Division, WSR-84-252 (1984).
[19] C.S. Caldwell, K.H. Puechl, F.D. Fisher, J. Roth, in: A.E. Kay, M.B. Waldron (Eds.), Plutonium 1965: Proceedings of the Third International Conference on Plutonium, London, 1965, Chapman and Hall for The Institute of Metals, London, 1967, p. 654.
[20] S. Glasstone, Sourcebook on Atomic Energy, D. Van Nostrand Company, Princeton, NJ, 1967.
[21] B. Bauefeld, D. Baither, U. Messerschmidt, M. Bartsch, I. Merkel, J. Am. Ceram. Soc. 76 (1993) 3163.
[22] G.E. Klein, 1. X-ray Examination of Ceramic Samples. 2. Operation of the Shielded X-ray Diffractometer, Oak Ridge National Laboratory, Oak Ridge, TN, Solid State Division Semiannual Progress Report, ORNL-1852 (1955).
[23] K.E. Sickafus, A.C. Larson, N. Yu, M. Nastasi, G.W. Hollenberg, F.A. Garner, R.C. Bradt, J. Nucl. Mater. 219 (1995) 128.
[24] M.C. Wittels, F.A. Sherrill, J. Appl. Phys. 27 (1956) 643.
[25] J.H. Crawford, M.C. Wittels, in: Second United Nations Conference on the Peaceful Uses of Atomic Energy, United nations, New York, Geneva, 1958, vol. 5, p. 300.
[26] M.C. Wittels, F.A. Sherrill, Phys. Rev. Lett. 3 (1959) 176.
[27] J. Adam, B. Cox, Phys. Rev. Lett. 3 (1959) 543.
[28] J. Adam, B. Cox, J. Nucl. Energy A 11 (1959) 31.
[29] T.S. Elleman, R.B. Price, D.N. Sunderman, Fission-Fragment-Induced Stresses in Ceramic Materials, Battelle Memorial Institute, Columbus, OH, BMI-1635 (1963).
[30] J.R. Johnson, Trans. Metall. Soc. AIME 212 (1959) 13.
[31] J.K. Dawson, B. Cox, R. Murdoch, R.G. Sowden, in Second United Nations Conference on the Peaceful Uses of Atomic Energy, United Nations, New York, Geneva, 1958, vol. 7, p. 22.
[32] R.M. Berman, M.L. Bleiberg, W. Yeniscavich, J. Nucl. Mater. 2 (1960) 129.
[33] F.W. Clinard Jr., D.L. Rohr, W.A. Ranken, J. Am. Ceram. Soc. 60 (1977) 287.
[34] E.L. Fleischer, M.G. Norton, M.A. Zaleski, W. Hertl, C.B. Carter, J.W. Mayer, J. Mater. Res. 6 (1991) 1905.
[35] N. Yu, K.E. Sickafus, P. Kodali, M. Nastasi, J. Nucl. Mater. 244 (1997) 266.
[36] C. Degueldre, P. Heimgartner, G. Ledergerber, N. Sasajima, K. Hojou, T. Muromura, L. Wang, W. Gong, R. Ewing, Mater. Res. Soc. Symp. Proc. 439 (1997) 625.
[37] K. Yasuda, M. Nastasi, K.E. Sickafus, C.J. Maggiore, N. Yu, Nucl. Instrum. and Meth. B 136–138 (1998) 499.
[38] N. Sasajima, T. Matsui, K. Hojou, S. Furuno, H. Otsu, K. Izui, T. Muromura, Nucl. Instrum. and Meth. Phy. Res. B 141 (1998) 487.
[39] K.E. Sickafus, C.J. Wetteland, N.P. Baker, N. Yu, R. Devanathan, M. Nastasi, N. Bordes, Mater. Sci. Eng. A 253 (1998) 78.
[40] N. Yu, K.E. Sickafus, M. Nastasi, Phil. Mag. Lett. 70 (1994) 235.
[41] E.L. Fleischer, W. Hertl, T.L. Alford, P. Borgensen, J.W. Mayer, J. Mater. Res. 5 (1990) 385.
[42] K.O. Legg, J.K.J. Cochran, H.F. Solnick-Legg, X.L. Mann, Nucl. Instrum. and Meth. Phys. Res. B 7&8 (1985) 535.
[43] J.G. Duh, Y.S. Wu, B.S. Chiou, J. Mater. Sci. Lett. 9 (1990) 916.
[44] J.G. Duh, Y.-S. Wu, J. Mater. Sci. 26 (1991) 6522.
[45] K.E. Sickafus, Hj. Matzke, K. Yasuda, P. Chodak III, R.A. Verrall, P.G. Lucuta, R.H. Andrews, A. Turos, R. Fromknecht, N.P. Baker, Nucl. Instrum. and Meth. B 141 (1998) 358.
[46] N. Yu, T.E. Levine, K.E. Sickafus, M. Nastasi, J.N. Mitchell, C.J. Maggiore, C.R. Evans, M.G. Hollander, J.R. Tesmer, W.J. Weber, J.W. Mayer, Nucl. Instrum. and Meth. B 118 (1996) 766.
[47] J.F. Ziegler, J.P. Biersack, U. Littmark, The Stopping and Range of Ions in Solids, Pergamon, New York, 1985.
[48] A.C. Larson, R.B. von Dreele, General Structure Analysis System, Los Alamos National Laboratory, Los Alamos, NM, LA-UR-86-748 (1986).
[49] Hj. Matzke, A. Turos, G. Linker, Nucl. Instrum. and Meth. Phys. Res. B 91 (1994) 294.
[50] Hj. Matzke, M. Kinoshita, J. Nucl. Mater. 247 (1997) 108.
[51] Hj. Matzke, P.G. Lucuta, T. Wiss, unpublished results (1997).
[52] A.J. Burggraaf, D. Scholten, B.A. van Hassel, Nucl. Instrum. and Meth. Phys. Res. B 32 (1988) 32.
[53] K. Bakker, H. Hein, R.J.M. Konings, R.R. van der Laan, Hj. Matzke, P. van Vlaanderen, J. Nucl. Mater. 252 (1998) 228.
[54] Hj. Matzke, Nucl. Instrum. and Meth. B 116 (1996) 121.

[55] S.J. Zinkle, Hj. Matzke, V.A. Skuratov, unpublished results (1998).
[56] K.E. Sickafus, R.J. Hanrahan Jr., K.J. McClellan, J.N. Mitchell, C.J. Wetteland, D.P. Butt, P. Chodak III, K.B. Ramsey, H.T. Blair, K. Chidester, Hj. Matzke, K. Yasuda, R.A. Verrall, N. Yu, Ceram. Bull. 78 (1999) 69.